nature medicine

Modulation of splicing catalysis for therapeutic targeting of leukemia with mutations in genes encoding spliceosomal proteins

Stanley Chun-Wei Lee[1,9], Heidi Dvinge[2,3,9], Eunhee Kim[1], Hana Cho[1], Jean-Baptiste Micol[1], Young Rock Chung[1], Benjamin H Durham[1], Akihide Yoshimi[1], Young Joon Kim[1], Michael Thomas[4], Camille Lobry[5], Chun-Wei Chen[6], Alessandro Pastore[1], Justin Taylor[1], Xujun Wang[6], Andrei Krivtsov[6], Scott A Armstrong[6,7], James Palacino[4], Silvia Buonamici[4], Peter G Smith[4], Robert K Bradley[2,3,10] & Omar Abdel-Wahab[1,8,10]

Mutations in genes encoding splicing factors (which we refer to as spliceosomal genes) are commonly found in patients with myelodysplastic syndromes (MDS) and acute myeloid leukemia (AML)[1–3]. These mutations recurrently affect specific amino acid residues, leading to perturbed normal splice site and exon recognition[4–6]. Spliceosomal gene mutations are always heterozygous and rarely occur together with one another, suggesting that cells may tolerate only a partial deviation from normal splicing activity. To test this hypothesis, we engineered mice to express a mutated allele of serine/arginine-rich splicing factor 2 (*Srsf2*^{P95H})—which commonly occurs in individuals with MDS and AML—in an inducible, hemizygous manner in hematopoietic cells. These mice rapidly succumbed to fatal bone marrow failure, demonstrating that *Srsf2*-mutated cells depend on the wild-type *Srsf2* allele for survival. In the context of leukemia, treatment with the spliceosome inhibitor E7107 (refs. 7,8) resulted in substantial reductions in leukemic burden, specifically in isogenic mouse leukemias and patient-derived xenograft AMLs carrying spliceosomal mutations. Whereas E7107 treatment of mice resulted in widespread intron retention and cassette exon skipping in leukemic cells regardless of *Srsf2* genotype, the magnitude of splicing inhibition following E7107 treatment was greater in *Srsf2*-mutated than in *Srsf2*-wild-type leukemia, consistent with the differential effect of E7107 on survival. Collectively, these data provide genetic and pharmacologic evidence that leukemias with spliceosomal gene mutations are preferentially susceptible to additional splicing perturbations *in vivo* as compared to leukemias without such mutations. Modulation of spliceosome function may thus provide a new therapeutic avenue in genetically defined subsets of individuals with MDS or AML.

Mutations in the spliceosomal genes *SRSF2*, *U2AF1*, and *SF3B1* are the most common class of mutations in patients with MDS[1–3] and occur across the entire spectrum of myeloid malignancies, including in 10–25% of patients with AML and in a higher proportion of patients with AML transformed from an antecedent MDS[9]. Recent studies revealed that heterozygous mutations in *SRSF2* (ref. 5), as well as *U2AF1* (ref. 4), drive hematopoietic stem–progenitor cell (HSPC) expansion in mice *in vivo* and that these mutations alter mRNA recognition in a sequence-specific manner[6]. However, it is still unclear why spliceosomal gene mutations occur in an exclusively heterozygous state in myeloid malignancies and why these mutations are mutually exclusive with one another. Moreover, given the frequency of these mutations and their early occurrence in myeloid malignancies[10–12], strategies to therapeutically target spliceosome-mutant malignancies are urgently needed.

We first took a genetic approach to test the hypothesis that cells carrying mutations in spliceosomal genes are sensitive to further perturbation of normal splicing. We engineered mice that conditionally expressed the *Srsf2*^{P95H} mutation in a hemizygous manner in the hematopoietic system (under the control of the *Mx1* promoter to drive the expression of Cre recombinase); conditional expression of the *Srsf2*^{P95H} allele could then be induced by administration of polyinosinic:polycytidylic acid (polyI:C). These mice enabled us to study the effects of deleting wild-type (WT) *Srsf2* and concomitantly activating expression of the *Srsf2*^{P95H} allele. *Mx1-Cre*$^{+}$*Srsf2*$^{+/fl}$ mice were crossed to *Srsf2*$^{P95H/+}$ mice to generate progeny that were WT for *Srsf2* (*Mx1-Cre*$^{+}$*Srsf2*$^{+/+}$), heterozygous knockout for *Srsf2* (*Mx1-Cre*$^{+}$*Srsf2*$^{+/fl}$), heterozygous for the *Srsf2*^{P95H} mutation (*Mx1-Cre*$^{+}$*Srsf2*$^{P95H/+}$), or hemizygous for the *Srsf2*^{P95H} mutation (*Mx1-Cre*$^{+}$*Srsf2*$^{P95H/fl}$) (**Supplementary Fig. 1a**). In noncompetitive

[1]Human Oncology and Pathogenesis Program, Memorial Sloan Kettering Cancer Center, New York, New York, USA. [2]Computational Biology Program, Public Health Sciences Division, Fred Hutchinson Cancer Research Center, Seattle, Washington, USA. [3]Basic Sciences Division, Fred Hutchinson Cancer Research Center, Seattle, Washington, USA. [4]H3 Biomedicine, Inc., Cambridge, Massachusetts, USA. [5]Institut National de la Santé et de la Recherche Medicale (INSERM) U1170, Institut Gustave Roussy, Villejuif, France. [6]Cancer Biology and Genetics Program, Memorial Sloan Kettering Cancer Center, New York, New York, USA. [7]Department of Pediatrics, Memorial Sloan Kettering Cancer Center, New York, New York, USA. [8]Leukemia Service, Department of Medicine, Memorial Sloan Kettering Cancer Center, New York, New York, USA. [9]These authors contributed equally to this work. [10]These authors jointly directed this work. Correspondence should be addressed to R.K.B. (rbradley@fredhutch.org) or O.A.-W. (abdelwao@mskcc.org).

Received 2 March; accepted 6 April; published online 2 May 2016; corrected online 11 May 2016 (details online); doi:10.1038/nm.4097

bone marrow (BM) transplantation assays, shortly after polyI:C administration, recipient mice reconstituted with BM mononuclear cells (MNCs) from hemizygous *Mx1-Cre*$^{+}$*Srsf2*$^{P95H/-}$ mice showed significantly shorter survival ($P = 0.004$) and severe BM aplasia (**Fig. 1a–c**) due to loss of HSPCs in the BM (**Supplementary Fig. 1b–f**), which was not observed in mice transplanted with BM MNCs from *Mx1-Cre*$^{+}$*Srsf2*$^{P95H/+}$, *Mx1-Cre*$^{+}$*Srsf2*$^{+/fl}$, or *Mx1-Cre*$^{+}$*Srsf2*$^{+/+}$ mice.

To determine the effect of hemizygous expression of the *Srsf2*^{P95H} allele on the transcriptome, we performed RNA-seq analysis on HSPCs (CD45.2^{+} lineage^{-} Sca1^{+}c-Kit^{+} (LSK) cells) isolated 2 weeks after polyI:C injection from mice that had been reconstituted with *Mx1-Cre*$^{+}$*Srsf2*$^{+/+}$, *Mx1-Cre*$^{+}$*Srsf2*$^{+/fl}$, *Mx1-Cre*$^{+}$*Srsf2*$^{P95H/+}$, or *Mx1-Cre*$^{+}$*Srsf2*$^{P95H/-}$ BM cells. We observed >3,000 dysregulated genes in *Srsf2*$^{P95H/-}$ HSPCs relative to all other groups, including >1.5-fold repression of many genes involved in hematopoietic stem cell self-renewal, including *Runx1*, *Erg*, and the entire *HoxA* cluster (**Fig. 1d** and **Supplementary Table 1**). Gene Ontology (GO) analysis of the differentially expressed genes in HSPCs from all four groups revealed that pathways related to cell migration, chemotaxis, cytokine production, and inflammatory responses were significantly overexpressed in *Mx1-Cre*$^{+}$*Srsf2*$^{P95H/-}$ relative to *Mx1-Cre*$^{+}$*Srsf2*$^{P95H/+}$ HSPCs (**Supplementary Fig. 1g**). We next tested whether hemizygous expression of *Srsf2*^{P95H} was associated with substantive alterations in splicing. We used Bayesian statistical methods (the MISO algorithm[13] and Wagenmakers's framework[14]) to quantify differential splicing of ~44,000 annotated alternative splicing events and ~170,000 constitutive splice junctions. We observed differential splicing of all classes of alternative splicing events, including competing 5′ and 3′ splice sites, cassette exons, and retained introns in *Mx1-Cre*$^{+}$*Srsf2*$^{P95H/-}$ cells, as well as alternative splicing and intron retention affecting normally constitutively spliced junctions. Although most splicing events remained unchanged, *Mx1-Cre*$^{+}$*Srsf2*$^{P95H/-}$ cells showed approximately two-fold more mis-splicing across all types of splicing events than did *Mx1-Cre*$^{+}$*Srsf2*$^{P95H/+}$ cells (**Supplementary Tables 1–3**).

We next tested whether increased mis-splicing in *Mx1-Cre*$^{+}$ *Srsf2*$^{P95H/-}$ cells was due to altered exon recognition. Heterozygous expression of the *SRSF2*^{P95H}, *SRSF2*^{P95L}, or *SRSF2*^{P95R} mutation alters SRSF2's recognition of specific exonic splicing enhancer (ESE) motifs and drives recurrent mis-splicing of transcripts for key hematopoietic regulators[5,15]. Quantification of the occurrence of ESE motifs within cassette exons that were differentially spliced in each genotype of LSK cells revealed a statistically significant preference for CCNG over GGNG ESE motifs in *Mx1-Cre*$^{+}$*Srsf2*$^{P95H/+}$ and *Mx1-Cre*$^{+}$*Srsf2*$^{P95H/-}$ cells (**Fig. 1e**), consistent with previous reports. CCNG motifs were enriched, and GGNG motifs were depleted, within differentially spliced cassette exons but not within flanking introns or exons (**Fig. 1f**).

To determine whether the cell lethality seen with *Srsf2*$^{P95H/-}$ hemizygosity was also present in the setting of leukemogenesis, we transduced *Srsf2*$^{P95H/fl}$ (control) or *Mx1-Cre*$^{+}$*Srsf2*$^{P95H/fl}$ (hemizygous) fetal liver cells with a green fluorescent protein (GFP)-expressing retroviral construct encoding the *KMT2A–MLLT3* fusion oncogene (also known as *MLL–AF9*) and then transplanted these cells into lethally irradiated recipient mice (**Supplementary Fig. 2a**). Although *Srsf2*$^{P95H/fl}$ control mice rapidly developed leukocytosis, anemia, thrombocytopenia, and elevated levels of donor-derived GFP^{+} cells, these features were substantially diminished in the hemizygous *Srsf2*$^{P95H/-}$ background (**Supplementary Fig. 2b–g**). Consistent with this observation, all of the mice from the control group eventually developed leukemia, whereas only five of ten *Srsf2*$^{P95H/-}$ mice succumbed to disease (**Supplementary Fig. 2h**). Moreover, leukemic cells in *Srsf2*$^{P95H/-}$ recipients uniformly escaped polyI:C-mediated recombination of the WT *loxP*-flanked (floxed) *Srsf2* allele, as compared to the cells in the blood samples taken from the same animals in the pre-leukemic state (**Supplementary Fig. 2i**). Overall, these observations revealed that *Srsf2*$^{P95H/+}$ cells specifically depend on the presence of the WT *Srsf2* allele for survival, even in the presence of a potent oncogene. These findings are consistent with the observation that mutations in genes encoding SRSF2 and other spliceosomal proteins are always heterozygous in individuals with MDS or AML, and they provide a potential explanation for the consistent heterozygous nature of spliceosomal gene mutations in cancer.

Having established, using mouse genetic models, that cells with spliceosomal gene mutations depend on WT splicing function, we hypothesized that spliceosome-mutant hematopoietic cells might display an altered response to pharmacologic inhibition of pre-mRNA splicing relative to their WT counterparts. To test this, we treated recipient mice with the splicing inhibitor E7107 (refs. 7,8). We first generated BM chimeras by transplanting *Srsf2*$^{+/+}$ or *Srsf2*$^{P95H/+}$ BM MNCs into lethally irradiated recipient mice. We then treated these mice with E7107 or vehicle starting at 6 months after transplantation (a time point at which stable engraftment of long-term hematopoiesis is expected) (**Supplementary Fig. 2j**). After five daily treatments of vehicle or E7107, we purified HSPCs (CD45.2^{+} lineage^{-} Sca1^{-} c-Kit^{+} cells) by flow cytometry and analyzed splicing and gene expression by RNA-seq. Ordination analysis by multidimensional scaling based on global cassette exon inclusion and global gene expression revealed that all of the vehicle-treated samples clustered together irrespective of *Srsf2* genotype, whereas the E7107-treated samples clustered on the basis of *Srsf2* genotype (**Fig. 2a**). These results indicate a differential gene expression and splicing response to E7107 treatment in *Srsf2*$^{P95H/+}$ hematopoietic cells as compared to their *Srsf2*$^{+/+}$ counterparts. We next examined whether this differential response to E7107 is due to the previously described altered ESE motif preference by mutant Srsf2. To do so, we performed a 'two-factor' analysis across two experimental parameters (vehicle versus E7107 and *Srsf2*$^{+/+}$ versus *Srsf2*$^{P95H/+}$) in which we systematically tested for preferential recognition of exons with different variants of the core SSNG (S = C or G) motif between each comparison (**Fig. 2b**). This analysis revealed that exons that are differentially spliced between the vehicle-treated *Srsf2*$^{+/+}$ and *Srsf2*$^{P95H/+}$ samples showed the expected difference in ESE motif preference (**Fig. 2b**, left), as previously published[5]. In contrast, there was no motif enrichment associated with the exons that were affected by E7107 in either *Srsf2*$^{+/+}$ or *Srsf2*$^{P95H/+}$ cells (**Fig. 2b**, top and bottom). However, we did observe that preferential recognition of exons with CCNG versus GGNG motifs in *Srsf2*$^{P95H/+}$ versus *Srsf2*$^{+/+}$ cells was weaker following E7107 treatment, and we identified a small subset of exons whose inclusion was affected in a genotype-dependent manner (**Fig. 2b**, right and **Supplementary Table 3**).

On the basis of these observations, we hypothesized that spliceosome-mutant leukemias might have greater sensitivity to pharmacologic inhibition of splicing than spliceosome-WT leukemias. Recent work[16] identified *SRSF2* mutations in ~10% of adult *MLL*-rearranged AMLs, suggesting that *MLL*-rearranged leukemias constitute a relevant system to study *SRSF2* mutations. By reanalyzing RNA-seq data[16] from human subjects with *MLL*-rearranged AML, we observed global alterations in splicing and ESE motif preference in *SRSF2*-mutated *MLL*-rearranged AML transcriptomes that are similar to those we previously reported in the *SRSF2*-mutated mouse model of MDS and in patients with myeloid leukemia[5] (**Fig. 2c,d**), suggesting that *SRSF2* mutations alter exon recognition in *MLL*-rearranged AML as

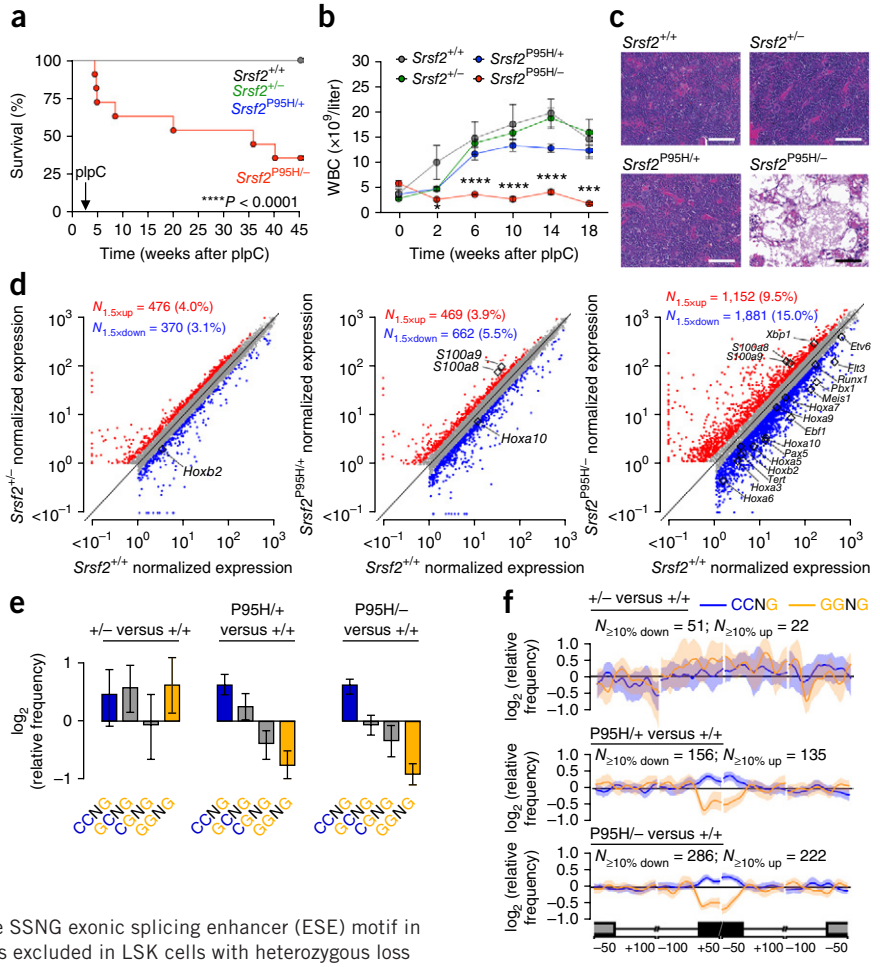

Figure 1 Spliceosome-mutant cells require the wild-type *Srsf2* allele for survival. (**a**) Kaplan–Meier survival curve of CD45.1 recipient mice transplanted with BM cells from control (*Mx1-Cre*$^{+}$*Srsf2*$^{+/+}$) mice or mice heterozygous (*Mx1-Cre*$^{+}$*Srsf2*$^{+/–}$) for the WT *Srsf2* allele, or mice heterozygous (*Mx1-Cre*$^{+}$*Srsf2*$^{P95H/+}$) or hemizygous (*Mx1-Cre*$^{+}$*Srsf2*$^{P95H/–}$) for the *Srsf2*^{P95H} (mutated) allele ($n = 10$ mice per group). Administration of polyI:C (plpC) was performed 4 weeks after transplantation. $^{****}P < 0.0001$ by Mantel–Cox log-ranked test. (**b**) White blood cell (WBC) counts in mice of each genotype over 18 weeks of noncompetitive transplantation ($n = 10$ mice per group). Error bars represent mean ± s.d. $^{***}P < 0.001$; $^{****}P < 0.0001$; by one-way analysis of variance (ANOVA). (**c**) Representative H&E-stained images of BM from CD45.1 recipient mice ($n = 10$ mice per group) that were transplanted with BM cells from the indicated mouse strains 8 weeks after transplantation. Scale bars, 200 µm. (**d**) Scatter plots comparing normalized expression of individual genes in lineage$^{–}$Sca1^{+}c-Kit^{+} (LSK) BM cells from *Mx1-Cre*$^{+}$*Srsf2*$^{+/–}$ (left), *Mx1-Cre*$^{+}$*Srsf2*$^{P95H/+}$ (middle), and *Mx1-Cre*$^{+}$*Srsf2*$^{P95H/–}$ (right) mice relative to those from WT control mice. Genes that were significantly dysregulated between comparisons (Bayes factor > 5; fold change > 1.5) are labeled in red (upregulated) and blue (downregulated), respectively. Differentially expressed genes of particular biological importance are highlighted in each plot. Units are transcripts per million. (**e**) Mean enrichment of all variants of the SSNG exonic splicing enhancer (ESE) motif in cassette exons that were differentially included versus excluded in LSK cells with heterozygous loss of (+/–), heterozygous mutation in (P95H/+), or hemizygous mutation in (P95H/–) *Srsf2* relative to the *Srsf2* control (+/+). Error bars indicate 95% confidence intervals estimated by bootstrapping. (**f**) Spatial distribution of CCNG and GGNG motifs adjacent to the sets of differentially spliced cassette exons analyzed in **e**. $N_{\geq 10\%\ down}$ and $N_{\geq 10\%\ up}$ indicate the number of exons that exhibited decreases or increases, respectively, in inclusion of absolute magnitude ≥10% in cells with the indicated genotypes relative to *Srsf2* control (+/+) cells. Shading indicates 95% confidence intervals by bootstrapping. The schematic (bottom) illustrates a portion of a metagene with the cassette exon (black box) separated from the upstream and downstream exons (gray boxes) by the beginning and end of the connecting introns. Horizontal axis indicates genomic coordinates defined with respect to the 5′ and 3′ splice sites where position 0 is the splice site itself. Vertical axis represents relative frequency of the indicated motifs over genomic loci containing cassette exons included versus those excluded in the indicated genotype comparisons (log scale).

expected. We therefore created an isogenic mouse leukemia model by retroviral overexpression of the *MLL–AF9* fusion oncogene in *Vav-Cre*$^{+}$*Srsf2*$^{+/+}$ or *Vav-Cre*$^{+}$*Srsf2*$^{P95H/+}$ BM cells (in which the *Vav* promoter drives hematopoietic-specific expression of the Cre recombinase) followed by transplantation into lethally irradiated recipient mice (**Supplementary Fig. 3a**). Overexpression of *MLL–AF9* in *Vav-Cre*$^{+}$*Srsf2*$^{+/+}$ or *Vav-Cre*$^{+}$*Srsf2*$^{P95H/+}$ BM cells resulted in fully penetrant AML with similar survival latencies and marked splenomegaly and hepatomegaly for both groups of mice (**Supplementary Fig. 3b,c**). Although *Srsf2*-mutated leukemias showed altered gene expression related to processes such as cell migration and response to external stimuli relative to their WT counterparts (**Supplementary Fig. 3d**), immunophenotype or histological and cytological analyses of BM, spleen, and liver revealed no obvious differences between the two genotypes (**Supplementary Fig. 3e–g**). We next examined the effects of pharmacological spliceosomal inhibition *in vivo*. To accomplish this, equal numbers of primary *MLL–AF9* leukemic cells from *Srsf2*$^{+/+}$ or *Srsf2*$^{P95H/+}$ mice were transplanted into secondary (2°) recipient mice to generate secondary leukemias, and the secondary recipient mice were then treated with either E7107 or vehicle (**Fig. 2e**). Ten days of intravenous (i.v.) administration of E7107 at 4 mg per kg of body weight per day (mg/kg/d) resulted in decreased disease burden—as assessed by peripheral blood leukocyte counts and the percentage of GFP^{+} cells (**Fig. 2f**), histological analyses (**Supplementary Fig. 3h**), and survival benefit in *Srsf2*$^{P95H/+}$ mice ($P = 0.001$)—whereas the same treatment regimen had no impact on overall survival of *Srsf2*$^{+/+}$ mice ($P = 0.621$) (**Fig. 2g**). E7107 treatment also improved anemia and thrombocytopenia in both *Srsf2*$^{+/+}$ or *Srsf2*$^{P95H/+}$ mice, with a slightly greater improvement observed in *Srsf2*$^{P95H/+}$ mice (**Supplementary Fig. 3i,j**).

To determine the mechanistic origins of the Srsf2-mutant-selective effects of E7107, we analyzed transcriptional changes after 5 d of E7107 treatment *in vivo* (**Fig. 3a**). Myeloid leukemic cells (marked by GFP^{+}Mac1^{+}) were purified from the BM of recipient mice exactly 3 h after the fifth dose of E7107 and subjected to RNA-seq analysis. E7107 exposure resulted in global splicing inhibition in both genotypes, typified by widespread intron retention and cassette exon skipping that is expected from inefficient splicing catalysis

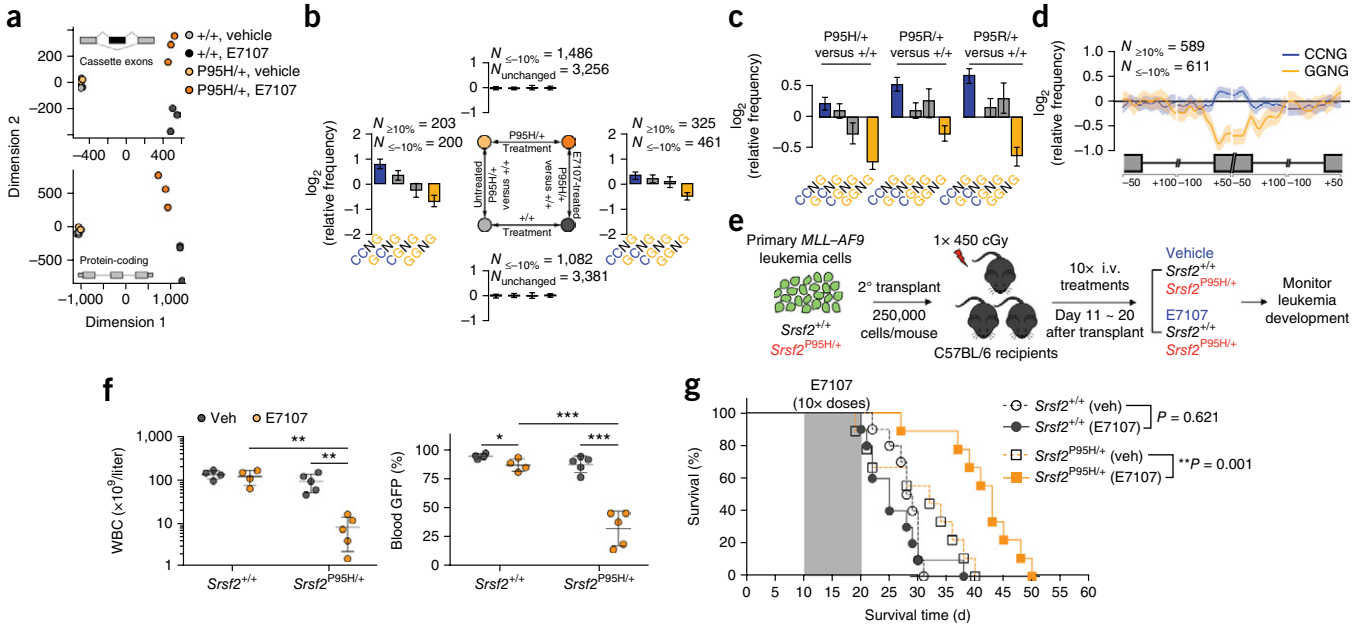

Figure 2 *SRSF2*-mutated myeloid leukemias are preferentially sensitive to pharmacologic modulation of splicing catalysis. (**a**) Multidimensional scaling using alternatively spliced cassette exons (top) and protein-coding genes (bottom) in LSK cells from the BM of *Mx1-Cre*$^{+}$*Srsf2*$^{P95H/+}$ and *Mx1-Cre*$^{+}$*Srsf2*$^{+/+}$ mice that were treated with vehicle or E7107 (4 mg/kg) for 5 d ($n = 3$ mice per group). (**b**) Mean enrichment of all variants of the SSNG ESE motif in cassette exons that were differentially included versus excluded in a two-factor comparison across all four experimental groups. $N_{\geq 10\%}$ and $N_{\leq -10\%}$ indicate the numbers of exons that exhibited increases and decreases in inclusion, respectively, of absolute magnitude ≥10% for the illustrated comparisons. For each comparison, enrichment was computed by comparing the indicated sets of exons (for example, cassette exons of each sequence from E7107-treated *Mx1-Cre*$^{+}$*Srsf2*$^{P95H/+}$ mice were compared with those from E7107-treated *Mx1-Cre*$^{+}$*Srsf2*$^{+/+}$ mice for the right-hand comparison). For sample comparisons where differentially spliced exons showing increased inclusion were not present (top and bottom), cassette exons that exhibited differential splicing of an absolute magnitude ≤10% were used as a background set to compute motif enrichment instead. The individual comparison that was used to generate each set of bar graphs is shown in the schema in the center of the figure. Error bars indicate 95% confidence intervals, as estimated by bootstrapping. (**c**) Mean enrichment of all variants of the SSNG ESE motif in individual *SRSF2*-mutant *MLL*-rearranged human AML samples relative to the median of 28 *SRSF2*-wildtype *MLL*-rearranged AML samples. Error bars indicate 95% confidence intervals estimated by bootstrapping. (**d**) Spatial distribution of CCNG and GGNG motifs along cassette exons that were included or excluded in the *SRSF2*-mutated samples relative to those in the median WT control among the *MLL*-rearranged AML samples. (**e**) Schematic of secondary transplantation experiments of mouse *MLL–AF9* leukemias in *Srsf2*$^{+/+}$ (*Vav-Cre*$^{+}$*Srsf2*$^{+/+}$) and *Srsf2*$^{P95H/+}$ (*Vav-Cre*$^{+}$*Srsf2*$^{P95H/+}$) backgrounds to test the effects of E7107 treatment *in vivo*. (**f**) WBC counts (left) and percentage of WBC cells expressing GFP (right) after 10 d of E7107 administration. (**g**) Kaplan–Meier survival curves of secondary recipient mice that were transplanted with *Srsf2*$^{+/+}$ or *Srsf2*$^{P95H/+}$ leukemic cells and treated with vehicle or E7107 (at 4 mg/kg) (*Srsf2*$^{+/+}$, $n = 10$ mice per group; *Srsf2*$^{P95H/+}$, $n = 9$ mice per group). Shaded area represents period of vehicle or E7107 dosing. Throughout, error bars represent mean ± s.d. $^{*}P < 0.05$; $^{**}P < 0.005$; $^{***}P < 0.001$; by Student's *t*-test.

(**Fig. 3b–d** (top and middle) and **Supplementary Fig. 4a**). Whereas E7107-induced splicing dysregulation was highly variable across animals in both *Srsf2*$^{P95H/+}$ and *Srsf2*$^{+/+}$ backgrounds, effects on global expression of protein coding genes was highly distinct between the genotypes (**Fig. 3b–d** (bottom) **Supplementary Fig. 4b,c**, and **Supplementary Table 1**). Moreover, the magnitude of splicing inhibition following E7107 treatment was more severe in *Srsf2*$^{P95H/+}$ versus *Srsf2*$^{+/+}$ mice, consistent with its differential effect on the survival of mice of these two genotypes (**Supplementary Fig. 4d**). GO analysis revealed that differentially expressed genes in *Srsf2*$^{P95H/+}$ relative to *Srsf2*$^{+/+}$ leukemic cells after E7107 treatment were enriched in biological pathways related to cytokine and immune signaling and to leukocyte activation and migration (**Supplementary Fig. 4e**).

Notably, genes involved in maintaining the leukemogenic programs in *MLL*-rearranged leukemias, including Dot1-like histone H3 methyltransferase (*Dot1l*) and Meis homeobox 1 (*Meis1*), were among the most differentially spliced genes in *Srsf2*$^{P95H/+}$ mice in response to E7107 treatment (**Fig. 3e** and **Supplementary Table 3**). Given the known importance of DOT1L to *MLL*-mediated leukemogenesis[17,18], we investigated the effects of E7107 treatment on *Dot1l* splicing further. Treatment with E7107 resulted in more pronounced exon skipping and intron retention within a region encoding the catalytic domain of the Dot1l protein in *MLL–AF9*;*Srsf2*$^{P95H/+}$ cells relative to their *MLL–AF9*;*Srsf2*$^{+/+}$ counterparts, which was readily detectable by RT–PCR and qRT–PCR during a time course of drug exposure (**Fig. 3f,g**). A similar increase in cassette exon skipping within *Meis1* was also observed by RT–PCR and qRT–PCR in *MLL–AF9*;*Srsf2*$^{P95H/+}$ cells as compared to that in *MLL–AF9*;*Srsf2*$^{+/+}$ cells (**Fig. 3f,g**). This increased mis-splicing in *Dot1l* and *Meis1* in the *Srsf2*-mutated background after E7107 exposure correlated with a mild decrease in Meis1 protein and Dot1l-mediated histone H3 Lys79 dimethylation (H3K79me2), indicating a reduction in Dot1l catalytic activity (**Supplementary Fig. 4f,g**). Conversely, exogenous re-expression of *DOT1L* cDNA resulted in a mild but consistent restoration in cellular proliferation in *MLL–AF9*;*Srsf2*$^{P95H/+}$ cells relative to that in *MLL–AF9*;*Srsf2*$^{+/+}$ cells after exposure to E7107 (**Supplementary Fig. 5a,b**). In contrast, *Meis1* overexpression was unable to rescue the inhibition of cell proliferation that was induced by E7107 treatment (**Supplementary Fig. 5c,d**). Of note, stable introduction of a previously identified point mutation in the gene splicing factor 3b, subunit 1 (*SF3B1*) known to cause E7107 resistance (*SF3B1*^{R1074H})[19] in *MLL–AF9*;*Srsf2*$^{P95H/+}$ cells (**Supplementary Fig. 5e–g**) rendered these cells almost completely insensitive to E7107, with a half-maximal inhibitory concentration (IC_{50}) nearly 300-fold greater than that

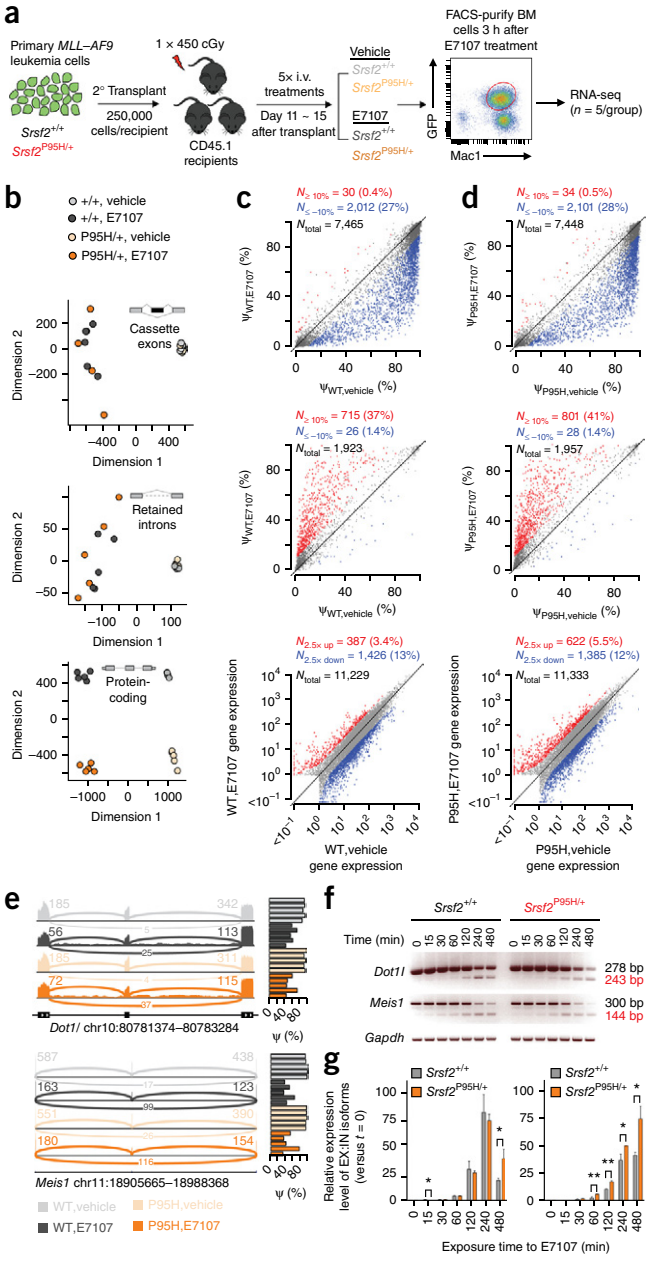

Figure 3 Splicing and gene expression changes in *Srsf2*-WT or *Srsf2*-mutated leukemia cells that were treated with E7107. (**a**) Schematic of secondary transplantation experimentation, with E7107 treatment for a defined amount of time followed by euthanization of the mice for RNA-seq analyses. Sublethally irradiated mice were transplanted with *MLL–AF9*;*Srsf2*$^{+/+}$ or *MLL–AF9*;*Srsf2*$^{P95H/+}$ primary leukemias, followed by treatment with E7107 (4 mg/kg/d) or vehicle for 5 d. GFP^{+}Mac1^{+} BM cells that were sorted 3 h after the fifth treatment were used for RNA-seq ($n = 5$ mice per group). (**b**) Multidimensional scaling analysis of all 20 mice from **a**, on the basis of alternatively spliced cassette exons ($N = 6,369$) (top), alternatively spliced retained introns ($N = 1,791$) (middle), and expressed protein-coding genes ($N = 9,339$) (bottom). (**c**,**d**) Scatter plots of cassette exon splicing (isoform ratios represented as percentage spliced in (PSI, Ψ) values) (top), retained introns (Ψ values) (middle), and gene expression (normalized expression values) (bottom) from *MLL–AF9*;*Srsf2*$^{+/+}$ (**c**) or *MLL–AF9*;*Srsf2*$^{P95H/+}$ (**d**) mice that were treated with vehicle or E7107. Percentages indicate the fraction of differentially spliced cassette exons or retained introns (inclusion rates increased or decreased by absolute magnitude ≥10% with $P < 0.01$) or the number of differentially expressed genes (fold change ≥ 2.5 with $P < 0.01$). Red and blue dots represent individual splicing events or coding genes whose expression is increased or decreased after treatment with E7107 versus vehicle, respectively. (**e**) Sashimi plots[28,29] across splice junctions surrounding differentially spliced cassette exons in *Dot1l* (top) and *Meis1* (bottom), with reads summarized across five replicate mice. Bar plots represent the percentage of spliced (ψ) cassette exon inclusion ratios across all samples. (**f**) Representative RT–PCR analysis of the effect of acute exposure to E7107 (10 nM) on splicing of *Dot1l* and *Meis1* in *MLL–AF9*;*Srsf2*$^{+/+}$ and *MLL–AF9*;*Srsf2*$^{P95H/+}$ leukemia cells *in vitro* ($n = 3$ biological replicates per group). (**g**) Quantification, by qRT–PCR, of the relative levels of exclusion (EX) and inclusion (IN) isoforms of *Dot1l* (left) and *Meis1* (right) following acute exposure to E7107 (10 nM) *in vitro* ($n = 3$ biological replicates per group). Error bars represent mean ± s.d. $^{*}P < 0.05$; $^{**}P < 0.01$; by Student's *t*-test.

of the parental or *SF3B1*^{WT}-overexpressing cells (**Supplementary Fig. 5h**). *SF3B1*^{R1074H}-expressing cells were also impervious to E7107-mediated inhibition of splicing (**Supplementary Fig. 5h**,**i**). Collectively, our data suggest that E7107 treatment induces phenotypic changes in *MLL–AF9* leukemia through aberrant splicing of multiple downstream targets, including *Dot1l* and *Meis1*, and provides genetic confirmation that E7107 affects cells through on-target inhibition of SF3B1.

Given that the above-mentioned data were generated in the specific context of *MLL*-rearranged mouse leukemias, we next sought to analyze the effect of splicing inhibition in the context of human AMLs in which endogenous *SRSF2* mutations also co-occur with a spectrum of mutations commonly found in myeloid leukemias. First, we tested the effect of E7107 on a previously described cassette exon inclusion event in the polycomb repressive complex (PRC) 2–subunit-encoding gene enhancer of zeste 2 (*EZH2*)[5] in human leukemia cell lines that were WT (TF-1) or mutated (K052) for *SRSF2*. RT–PCR and qRT–PCR analyses revealed that E7107 treatment inhibits SRSF2 mutant-specific *EZH2* mis-splicing in a dose-dependent manner (**Fig. 4a**,**b**). Next, to evaluate *in vivo* drug effects in primary human AMLs, we generated patient-derived xenografts (PDXs) from a cohort of patients with primary AML ($n = 2$ without a spliceosomal gene mutation, $n = 3$ with a spliceosomal gene mutation; **Supplementary Table 4**). Primary leukemia cells from each individual patient were transplanted via tail-vein injection into ten adult immunodeficient NOD–Scid *Il2rg*^{null} (NSG) mice. After the human CD45^{+} cells reached >25% of the total cells in the BM of NSG mice (median of 86 d after transplantation; range 62–148 d), mice were treated with E7107 (4 mg/kg/d) or vehicle for 10 d (**Fig. 4c**). In each PDX model, targeted genomic analysis of purified human leukemic cells from the BM confirmed faithful engraftment of the major leukemic clones that were found in the primary patient samples (**Supplementary Fig. 6a**) and revealed that spliceosomal gene mutations were present in the major leukemic clones following E7107 treatment *in vivo* (**Supplementary Fig. 6b**). All spliceosome-mutant AML PDXs showed significant reductions in human leukemic burden in response to E7107 treatment, whereas the response in AML cells that were WT for splicing was less robust (**Fig. 4d**,**e**). Further examination revealed that two of three spliceosome-mutant AMLs had a substantial decrease in hCD45^{+} hCD34^{+} HSPC subsets (**Supplementary Fig. 6c**). In contrast, AMLs that were WT for splicing showed less substantial reductions in leukemic cells, as well as in hCD45^{+} hCD34^{+} cell subsets (**Fig. 4d**,**e** and **Supplementary Fig. 6c–e**). Although E7107 treatment resulted in reduced cell proliferation 3 h after treatment *in vivo* regardless of spliceosome mutational status (**Fig. 4f**), the preferential sensitivity to E7107 in spliceosome-mutant AML was associated with substantially increased apoptosis only in spliceosome-mutant PDX samples (**Fig. 4g**,**h** and **Supplementary Fig. 6f**). These data establish

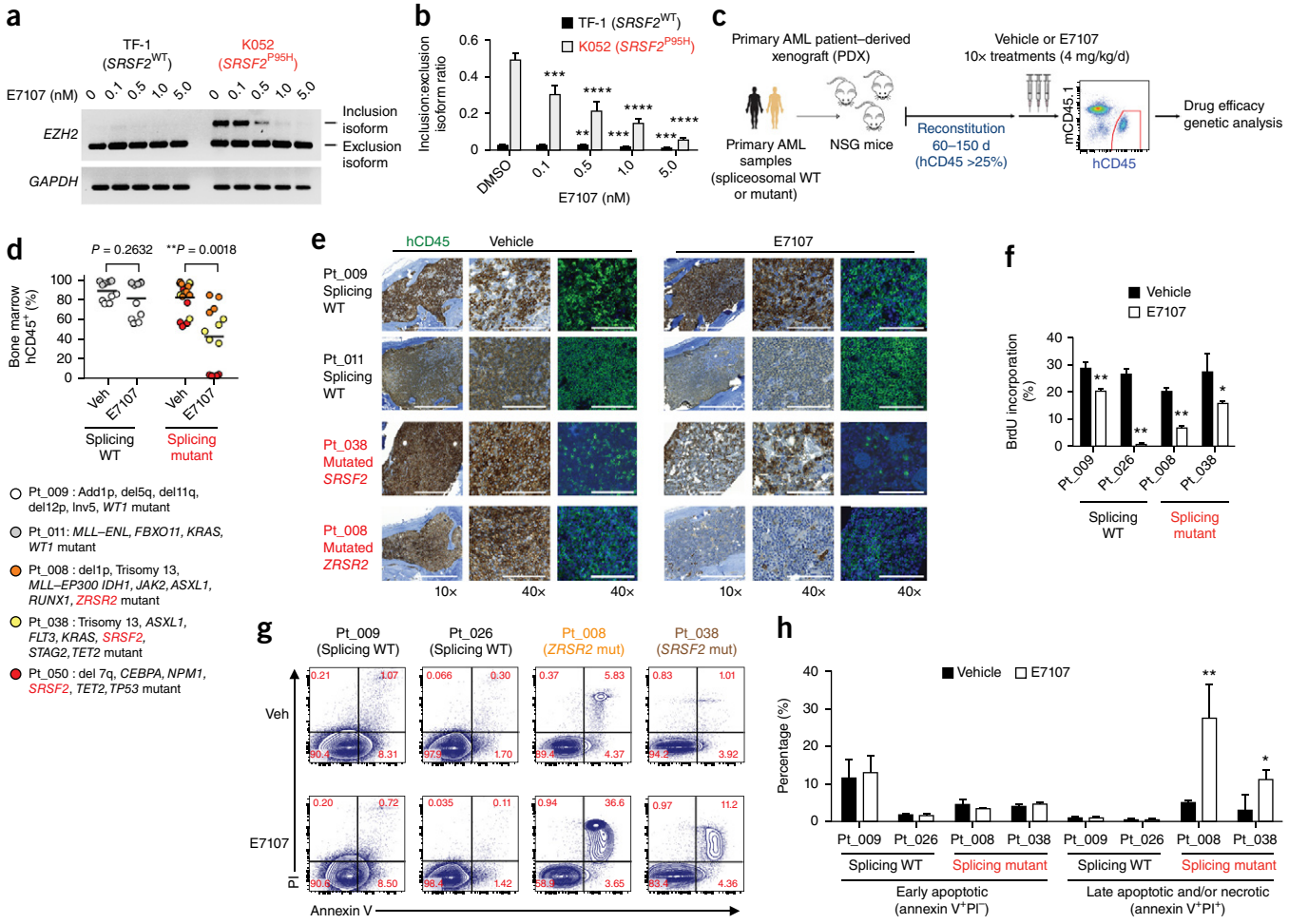

Figure 4 Preferential sensitivity of primary human leukemias to pharmacologic modulation of splicing *in vivo* with E7107. (**a**,**b**) Representative RT–PCR analysis (**a**) and quantification, by qRT–PCR, (**b**) of the effect of E7107 exposure (6 h), relative to DMSO treatment, on expression of a cassette exon inclusion isoform ('poison' exon) of *EZH2* in leukemia cell lines that are either WT (TF-1) or mutated (K052) for *SRSF2*. (**c**) Schema of patient-derived xenograft (PDX) experiments, using engraftment of primary human AML samples (either WT or mutated for spliceosomal genes) into NSG mice. (**d**) Quantification of human CD45 chimerism (hCD45+) (from PDX samples from patients (Pts.) with AML who have (indicated in color) or do not have mutations in spliceosomal genes) in the BM of NSG recipient mice after 10 d of treatment with vehicle or E7107 (4 mg/kg/d). Each circle represents the hCD45 value for an individual NSG mouse, and each color represents the PDX from a specific patient. Mutational data for each patient are listed below the graph. (**e**) Representative immunohistochemical and immunofluorescence analysis for hCD45 in BM sections of recipient mice shown in **d**. Scale bars, 200 µm (10× images) and 50 µm (40× images). (**f**) BM hCD45+ cells in S phase, on the basis of *in vivo* BrdU incorporation after 5 d of treatment with E7107 (4 mg/kg/d) or vehicle. (**g**,**h**) Representative FACS plots of annexin V and propidium iodide (PI) staining of hCD45 cells following 5 d of E1707 (4 mg/kg/d) (bottom) or vehicle (top) treatment *in vivo* (**g**) and quantification of annexin V+PI– or annexin V+PI+ hCD45+ cells (**h**). In **f**,**g**,**h**: for Pt_009, $n = 3$ mice; for Pt_026, $n = 2$ mice; for Pt_008, $n = 4$ mice; for Pt_038, $n = 3$ mice. Throughout, error bars represent mean ± s.d. $^{*}P < 0.05$; $^{**}P < 0.01$; $^{***}P < 0.001$; $^{****}P < 0.0001$; by Student's *t*-test.

a relationship between sensitivity to E7107 and the mutational status of spliceosomal genes in primary AMLs.

Whereas splicing is an essential process required for the normal function of all mammalian cells, here we provide both genetic and pharmacologic evidence that SRSF2-mutant leukemias are preferentially sensitive to splicing modulation *in vivo* relative to SRSF2-WT leukemias. Genomic and biological analyses of cells expressing mutant SRSF2 in the absence of the WT protein indicated that the *SRSF2* mutation, despite being selected for in human leukemia[1,5], is unable to, on its own, support gene expression and splicing patterns required for hematopoiesis. The sensitivity of *SRSF2*-mutated leukemias to loss of the WT *SRSF2* allele was mirrored by the exposure of leukemias bearing heterozygous *SRSF2* mutations to E7107, an inhibitor of splicing[8]. Because mutations affecting the spliceosomal proteins SF3B1 and U2AF1 are also found in an exclusively heterozygous context, it will be important to determine whether the broad range of malignancies carrying diverse spliceosomal gene mutations may prove similarly sensitive to pharmacologic perturbation of normal splicing catalysis.

Given the high frequency of *SRSF2* mutations across myeloid malignancies[1,20,21], the adverse outcome associated with *SRSF2* mutations[20,22,23], and the need for novel therapeutic approaches for these disorders, the data provided here have important therapeutic implications for patients with MDS and AML who have genetic alterations in *SRSF2*. E7107 is one of a host of structurally distinct splicing inhibitors, all of which hinder normal splicing in a similar manner by inhibiting SF3B1 function[24,25]. The only such compound that has been tested in humans to date is E7107, for which there are two completed phase 1 dose-escalation studies for patients with advanced

solid tumors. In patients treated with E7107, inhibition of splicing was observed during dose escalation, and the dose-limiting toxicity was primarily gastrointestinal related; however, visual impairment was reported in 3/66 patients[26,27]. The data presented here demonstrate that SF3B1 inhibition has therapeutic potential for the treatment of malignancies with *SRSF2* mutations; clinical studies with newly identified SF3B1 inhibitors will be essential to define the safety and therapeutic efficacy of this approach in patients. Moreover, ongoing efforts to understand how pharmacological inhibitors of splicing alter the constellation of proteins that directly or indirectly bind to SF3B1, and how mutations affecting splicing factors might alter protein–protein interactions, will facilitate the future development of compounds with heightened specificity for cells with mutant spliceosomes.

METHODS

Methods and any associated references are available in the online version of the paper.

Accession codes. Gene Expression Omnibus: all newly generated RNA-seq data were deposited under accession number GSE74064.

Note: Any Supplementary Information and Source Data files are available in the online version of the paper.

ACKNOWLEDGMENTS

This work was supported by the Leukemia and Lymphoma Society (S.C.-W.L. and O.A.-W.), the US Department of Defense Breast Cancer Research Program grant W81XWH-14-1-0044 (H.D.), the US Department of Defense Bone Marrow Failure Research Program grants BM150092 (O.A.-W.) and W81XWH-12-1-0041 (R.K.B. and O.A.-W.), the Worldwide Cancer Research Fund (E.K.), the Fondation de France (J.-B.M.), the American Society of Hematology (B.H.D. and O.A.-W.), the Edward P. Evans Foundation (R.K.B. and O.A.-W.), the US National Institutes of Health (NIH)-NHLBI grant R01 HL128239 (R.K.B. and O.A.-W.), the NIH–NCI grant 1K08CA160647-01 (O.A.-W.), the Ellison Medical Foundation grant AG-NS-1030-13 (R.K.B.), the Damon Runyon Foundation (R.K.B. and O.A.-W.), the NIH–NIDDK grant R01 DK103854 (R.K.B.), the Starr Foundation grant I8-A8-075 (O.A.-W.), the Josie Robertson Investigator Program (O.A.-W.), the Mr. William H. Goodwin and Mrs. Alice Goodwin Commonwealth Foundation for Cancer Research (O.A.-W.), and the Experimental Therapeutics Center of MSKCC (O.A.-W.).

AUTHOR CONTRIBUTIONS

S.C.-W.L., H.D., E.K., R.K.B., and O.A.-W. designed the study; S.C.-W.L., E.K., H.C., Y.R.C., J.-B.M., B.H.D., A.Y., Y.J.K., C.-W.C., A.P., J.T., X.W., A.K., S.A.A., and O.A.-W. performed experiments; H.D. and R.K.B. performed RNA-seq analysis; M.T., J.P., S.B., and P.G.S. provided E7107 and advice with drug-dosing experiments; and S.C.-W.L., H.D., E.K., C.L., R.K.B., and O.A.-W. prepared the manuscript with help from all co-authors.

COMPETING FINANCIAL INTERESTS

The authors declare competing financial interests: details are available in the online version of the paper.

1. Yoshida, K. *et al.* Frequent pathway mutations of splicing machinery in myelodysplasia. *Nature* **478**, 64–69 (2011).
2. Papaemmanuil, E. *et al.* Somatic *SF3B1* mutation in myelodysplasia with ring sideroblasts. *N. Engl. J. Med.* **365**, 1384–1395 (2011).
3. Graubert, T.A. *et al.* Recurrent mutations in the *U2AF1* splicing factor in myelodysplastic syndromes. *Nat. Genet.* **44**, 53–57 (2012).
4. Shirai, C.L. *et al.* Mutant U2AF1 expression alters hematopoiesis and pre-mRNA splicing *in vivo*. *Cancer Cell* **27**, 631–643 (2015).
5. Kim, E. *et al. SRSF2* mutations contribute to myelodysplasia by mutant-specific effects on exon recognition. *Cancer Cell* **27**, 617–630 (2015).
6. Ilagan, J.O. *et al. U2AF1* mutations alter splice site recognition in hematological malignancies. *Genome Res.* **25**, 14–26 (2015).
7. Folco, E.G., Coil, K.E. & Reed, R. The antitumor drug E7107 reveals an essential role for SF3b in remodeling U2 snRNP to expose the branch point-binding region. *Genes Dev.* **25**, 440–444 (2011).
8. Kotake, Y. *et al.* Splicing factor SF3b as a target of the antitumor natural product pladienolide. *Nat. Chem. Biol.* **3**, 570–575 (2007).
9. Lindsley, R.C. *et al.* Acute myeloid leukemia ontogeny is defined by distinct somatic mutations. *Blood* **125**, 1367–1376 (2015).
10. Genovese, G., Jaiswal, S., Ebert, B.L. & McCarroll, S.A. Clonal hematopoiesis and blood-cancer risk. *N. Engl. J. Med.* **372**, 1071–1072 (2015).
11. Xie, M. *et al.* Age-related mutations associated with clonal hematopoietic expansion and malignancies. *Nat. Med.* **20**, 1472–1478 (2014).
12. Genovese, G. *et al.* Clonal hematopoiesis and blood-cancer risk inferred from blood DNA sequence. *N. Engl. J. Med.* **371**, 2477–2487 (2014).
13. Katz, Y., Wang, E.T., Airoldi, E.M. & Burge, C.B. Analysis and design of RNA sequencing experiments for identifying isoform regulation. *Nat. Methods* **7**, 1009–1015 (2010).
14. Wagenmakers, E.J., Lodewyckx, T., Kuriyal, H. & Grasman, R. Bayesian hypothesis testing for psychologists: a tutorial on the Savage–Dickey method. *Cognit. Psychol.* **60**, 158–189 (2010).
15. Zhang, J. *et al.* Disease-associated mutation in *SRSF2* misregulates splicing by altering RNA-binding affinities. *Proc. Natl. Acad. Sci. USA* **112**, E4726–E4734 (2015).
16. Lavallée, V.P. *et al.* The transcriptomic landscape and directed chemical interrogation of *MLL*-rearranged acute myeloid leukemias. *Nat. Genet.* **47**, 1030–1037 (2015).
17. Daigle, S.R. *et al.* Selective killing of mixed lineage leukemia cells by a potent small-molecule DOT1L inhibitor. *Cancer Cell* **20**, 53–65 (2011).
18. Bernt, K.M. *et al. MLL*-rearranged leukemia is dependent on aberrant H3K79 methylation by DOT1L. *Cancer Cell* **20**, 66–78 (2011).
19. Yokoi, A. *et al.* Biological validation that SF3b is a target of the antitumor macrolide pladienolide. *FEBS J.* **278**, 4870–4880 (2011).
20. Papaemmanuil, E. *et al.* Clinical and biological implications of driver mutations in myelodysplastic syndromes. *Blood* **122**, 3616–3627, quiz 3699 (2013).
21. Bejar, R. *et al.* Validation of a prognostic model and the impact of mutations in patients with lower-risk myelodysplastic syndromes. *J. Clin. Oncol.* **30**, 3376–3382 (2012).
22. Zhang, S.J. *et al.* Genetic analysis of patients with leukemic transformation of myeloproliferative neoplasms shows recurrent *SRSF2* mutations that are associated with adverse outcome. *Blood* **119**, 4480–4485 (2012).
23. Vannucchi, A.M. *et al.* Mutations and prognosis in primary myelofibrosis. *Leukemia* **27**, 1861–1869 (2013).
24. Effenberger, K.A., Urabe, V.K., Prichard, B.E., Ghosh, A.K. & Jurica, M.S. Interchangeable SF3B1 inhibitors interfere with pre-mRNA splicing at multiple stages. *RNA* **22**, 350–359 (2016).
25. Bonnal, S., Vigevani, L. & Valcárcel, J. The spliceosome as a target of novel antitumor drugs. *Nat. Rev. Drug Discov.* **11**, 847–859 (2012).
26. Eskens, F.A. *et al.* Phase 1 pharmacokinetic and pharmacodynamic study of the first-in-class spliceosome inhibitor E7107 in patients with advanced solid tumors. *Clin. Cancer Res.* **19**, 6296–6304 (2013).
27. Hong, D.S. *et al.* A phase 1, open-label, single-arm, dose-escalation study of E7107, a precursor messenger ribonucleic acid (pre-mRNA) splicesome inhibitor, administered intravenously on days 1 and 8 every 21 days to patients with solid tumors. *Invest. New Drugs* **32**, 436–444 (2014).
28. Katz, Y. *et al.* Quantitative visualization of alternative exon expression from RNA-seq data. *Bioinformatics* **31**, 2400–2402 (2015).
29. Thorvaldsdóttir, H., Robinson, J.T. & Mesirov, J.P. Integrative genomics viewer (IGV): high-performance genomics data visualization and exploration. *Brief. Bioinform.* **14**, 178–192 (2013).

ONLINE METHODS

Mice. All mice were housed at Memorial Sloan Kettering Cancer Center (MSKCC). All animal procedures were completed in accordance with the Guidelines for the Care and Use of Laboratory Animals[30] and were approved by the Institutional Animal Care and Use Committees at MSKCC. The number of mice in each experiment was chosen to provide 90% statistical power with a 5% error level. Generation and genotyping of the *Srsf2*$^{P95H/+}$ conditional knock-in mice as well as the *Srsf2* conditional-knockout mice (both on the C57BL/6 background) were as previously described[5,31]. For *MLL–AF9* BM transplantation assays, *Srsf2*$^{P95H/+}$ and littermate control mice were crossed to *Vav-Cre* transgenic mice[32].

Peripheral blood analysis. Blood was collected by retro-orbital bleeding using heparinized microhematocrit capillary tubes (Thermo Fisher Scientific). Automated peripheral blood counts were obtained using an IDEXX ProCyte Dx Hematology Analyzer. Differential blood counts were scored on blood smears stained using Wright–Giemsa stain and visualized using an Axio Observer A1 microscope.

Histological analyses. Mice were euthanized and autopsied, and the dissected tissue samples were fixed in 4% paraformaldehyde, dehydrated, and embedded in paraffin. Paraffin blocks were sectioned at 4 μm and stained with hematoxylin and eosin (H&E). Images were acquired using an Axio Observer A1 microscope (Carl Zeiss) or scanned using a MIRAX Scanner (Zeiss).

Bone marrow (BM) transplantation assays. Freshly dissected femora and tibiae were isolated from *Mx1-Cre*$^{+}$*Srsf2*$^{+/+}$, *Mx1-Cre*$^{+}$*Srsf2*$^{+/fl}$, *Mx1-Cre*$^{+}$*Srsf2*$^{P95H/+}$, or *Mx1-Cre*$^{+}$*Srsf2*$^{P95H/fl}$ CD45.2^{+} mice of both sexes. BM was flushed with a 3-ml insulin syringe into cold PBS (without Ca^{2+} and Mg^{2+}), supplemented with 2% bovine serum albumin, to generate single-cell suspensions. BM cells were pelleted by centrifugation at 1,500 r.p.m. for 5 min, and the red blood cells (RBCs) were lysed in ammonium chloride–potassium bicarbonate lysis (ACK) buffer for 5 min on ice. After centrifugation, cells were resuspended in PBS with 2% BSA, passed through a 40-μm cell strainer, and counted. For competitive transplantation experiments, 0.5×10^6 BM cells from *Mx1-Cre*$^{+}$*Srsf2*$^{+/+}$, *Mx1-Cre*$^{+}$*Srsf2*$^{+/fl}$, *Mx1-Cre*$^{+}$*Srsf2*$^{P95H/+}$, or *Mx1-Cre*$^{+}$*Srsf2*$^{P95H/fl}$ CD45.2^{+} mice were mixed with 0.5×10^6 wild-type CD45.1^{+} support BM and transplanted via tail vein injection into 6-week-old lethally irradiated (900 cGy) female CD45.1^{+} recipient mice. To activate the conditional alleles, mice were treated with three doses of polyinosinic:polycytidylic acid (polyI:C; 12 mg/kg/d; GE Healthcare) every second day via intraperitoneal injection. Peripheral blood chimerism was assessed every 4 weeks by flow cytometry. For noncompetitive transplantation experiments, 1×10^6 total BM cells from *Mx1-Cre*$^{+}$*Srsf2*$^{+/+}$, *Mx1-Cre*$^{+}$*Srsf2*$^{+/fl}$, *Mx1-Cre*$^{+}$*Srsf2*$^{P95H/+}$, or *Mx1-Cre*$^{+}$*Srsf2*$^{P95H/fl}$ CD45.2^{+} mice were injected into lethally irradiated (900 cGy) CD45.1^{+} recipient mice. Peripheral blood chimerism was assessed as described for competitive transplantation experiments. Additionally, for each bleeding, whole-blood cell counts were measured on an automated blood analyzer. Animals that failed to engraft (<1% CD45.2 chimerism in peripheral blood) or were lost due to poly(I:C) toxicity were excluded from analysis.

Xenografts of primary human AML samples. Studies were approved by the Institutional Review Boards of Memorial Sloan Kettering Cancer Center and Fred Hutchinson Cancer Research Center and conducted in accordance to the Declaration of Helsinki protocol. Primary human AML samples derived from whole peripheral blood or BM MNCs were depleted of CD3^{+} T lymphocytes and transplanted via tail vein injection into 6-week-old NOD–Scid *Il2rg*^{null} (NSG) mice (Jackson Laboratory) conditioned with 200 cGy of gamma irradiation. Mice were bled monthly to assess the presence of human CD45^{+} cells in the blood. If hCD45^{+} was >1%, then BM aspiration was performed to assess BM hCD45 chimerism.

Retroviral transduction and transplantation of primary hematopoietic cells. *Vav-Cre*$^{+}$*Srsf2*$^{+/+}$ and *Vav-Cre*$^{+}$*Srsf2*$^{P95H/+}$ mice were treated with a single dose of 5-fluorouracil (150 mg/kg) followed by BM harvest from the femora, tibiae and hip bones 6 d later. RBCs were removed by ACK lysis buffer, and nucleated BM cells were transduced with viral supernatants containing murine stem cell virus (MSCV)-driven *MLL–AF9* fusion oncogene in a construct tagged with *GFP* reported from an internal ribosomal entry site (MSCV-*MLL–AF9*-IRES-*GFP*) for 2 d in Iscove's modified Dulbecco's medium (IMDM) with 15% fetal calf serum (FCS) supplemented with mouse stem cell factor (mSCF) (25 ng/ml), mouse interleukin (IL)-3 (10 ng/ml) and mouse IL-6 (10 ng/ml), followed by injection of ~400,000 cells per recipient mouse via tail vein injection into lethally irradiated (900 cGy) CD45.1 mice. For secondary transplantation experiments, 6-week-old, sublethally irradiated (450 cGy) C57/BL6 recipient mice were injected with 250,000 primary *MLL–AF9* leukemic cells. For *Srsf2* hemizygous rescue experiments, *Srsf2*$^{P95H/fl}$ and *Mx1-Cre*$^{+}$*Srsf2*$^{P95H/fl}$ fetal liver cells (embryonic day (E) 12.5–E14.5) were c-Kit-enriched using CD117 MicroBeads (MACS, Miltenyi Biotec) and transduced with viral supernatants containing MSCV-*MLL–AF9*-IRES-GFP twice for 2 d in IMDM with 15% FCS supplemented with mSCF (100 ng/ml), mouse thrombopoietin (mTPO; 50 ng/ml), mouse FLT3 ligand (mFLT3-L; 5 ng/ml), and mouse IL-6 (10 ng/ml), followed by tail vein injection of ~500,000 cells into lethally irradiated (900 cGy) CD45.1 recipient mice. All cytokines were purchased from R&D Systems.

Flow cytometry analyses and antibodies. Surface marker staining of hematopoietic cells was performed by first lysing cells with ACK lysis buffer and then washing the cells with ice-cold PBS. Cells were stained with antibodies in PBS with 2% BSA for 30 min on ice. For hematopoietic stem and progenitor cell staining, cells were stained with a specific lineage-positive antibody cocktail, including antibodies specific for B220 (RA3-6B2), CD3 (17A2), CD4 (RM4-5), Gr-1 (RB6-8C5), Mac1 (M1/70), NK1.1 (PK136), and Ter119 (all from BioLegend), allowing for mature lineage exclusion from the analysis. Cells were also stained with monoclonal antibodies against c-Kit (2B8), Sca1 (D7), Fc-γRII and Fc-γRIII (2.4G2), CD34 (RAM34), CD45.1 (A20), CD45.2 (104), CD48 (HM48-1), and CD150 (9D1) (all from eBioscience). The composition of mature hematopoietic cell lineages in the BM, spleen and peripheral blood was assessed using a combination of Mac1, Gr-1, B220, CD19, CD4 and CD8 staining. For analysis of human cell populations in mouse xenograft experiments, BM mononuclear cells and peripheral blood mononuclear cells were stained with a combination of antibodies against hCD3 (SK7), hCD19 (HIB19), hCD33 (WM-53), hCD34 (4H11), hCD38 (HIT2), and hCD45 (HI30) (all from eBioscience). Antibodies against mouse CD45.1 (A20) and Ter119 were used to exclude host-derived cells. DAPI was used to exclude dead cells. The final staining volume was 100 μl, and the final concentration for all antibodies used was 1:200, except for CD34 (1:50), c-Kit (1:100), and CD150 (1:100). For *in vivo* apoptosis experiments, BM cells were harvested from NSG mice 3 h after E7107 treatment. Cells were stained with an allophycocyanin (APC)-conjugated annexin V antibody in annexin V binding buffer (BD Pharmingen) to detect cells undergoing apoptosis, according to the manufacturer's instructions. For assessment of the effect of E7107 treatment on cell cycle status *in vivo*, 5-bromo-2′-deoxyuridine (BrdU; 0.1 mg per g body weight (mg/g)) was administered via intraperitoneal injection to NSG mice 24 h before drug treatment. BM cells were harvested 3 h after E7107 treatment, and the detection of BrdU incorporation was performed following the manufacturer's instructions (BD Pharmingen) Propidium iodide (PI) was used as a counter stain in both the annexin V and BrdU experiments. All FACS sorting was performed on FACS Aria, and analysis was performed on an LSRII or LSR Fortessa (BD Biosciences). For western blotting, the following antibodies to the following proteins were used: H3K79me2 (Abcam; Ab-3594), histone H3 (Cell Signaling Technologies; D1-H2), Meis1 (Abcam; Ab-124686), Sf3b1/Sap-155 (MBL; D221-3), Flag-M2 (Sigma-Aldrich; F-1084) and β-actin (Sigma-Aldrich; A-5441). All primary antibodies for western blotting were diluted to a final concentration of 1:1,000, in either 5% BSA (Sigma-Aldrich) in 0.05% TBS–Tween 20 (TBS-T) or 5% skim milk in 0.05% TBS-T.

Administration of spliceosome modulator E7107 *in vitro* and *in vivo*. For all *in vitro* experiments E7107 was dissolved in DMSO. For drug-sensitivity studies, cells were exposed to E7107 from a range of 10 μM to 0.05 nM. For *in vivo* administration, E7107 was dissolved in vehicle (10% ethanol and 4% Tween-80 in sterile PBS) and administered via intravenous (i.v.) injection at

4 mg/kg/d. For drug-efficacy studies, randomization was done by conducting WBC analysis before the start of drug administration and confirming that WBC count averages were equivalent in treatment and vehicle groups. All mice received ten consecutive doses of E7107. No blinding was done in the *in vivo* drug studies or in data analysis. For RNA-seq analysis in the mouse *MLL–AF9* leukemia model, five consecutive doses of E7107 were administered to the mice. The mice were euthanized 3 h after receiving the last dose, and BM Mac1$^+$ GFP$^+$ cells were purified by flow cytometry.

Cell culture. K052 leukemia cells were purchased from the Japanese Collection of Research Bioresources (JCRB) Cell Bank (JCRB0123) and were cultured in RPMI medium (made in-house at MSKCC) with 10% FCS. TF-1 cells were purchased from Deutsche Sammlung von Mikroorganismen und Zellkulturen (DSMZ; ACC344); these cells were cultured in RPMI medium with 10% FCS supplemented with human granulocyte–macrophage colony-stimulating factor (hGM-CSF) (R&D Systems; 5 ng/ml). Primary mouse *MLL–AF9* leukemia cell lines were generated from BM cells of leukemia-bearing mice and maintained in IMDM with 15% FCS, supplemented with L-glutamine, mSCF (20 ng/ml), mouse IL-3 (10 ng/ml), and mouse IL-6 (10 ng/ml). All cell lines have been tested for mycoplasma contamination and authenticated to confirm the status of the *SRSF2* mutation.

MSCV-Flag-Bio-*DOT1L*-Puro, MSCV-*Meis1*-IRES-Puro, and MSCV-IRES-Puro constructs were used for overexpression studies. Retroviral supernatants were produced by transfecting 293 GPII cells (Clontech Laboratories) with cDNA constructs and the packaging plasmid VSV.G using XtremeGene9 (Roche) and were used to transduce *MLL–AF9* leukemic cells in the presence of polybrene (5 μg/ml), followed by puromycin selection (1 μg/ml; Invitrogen) for successfully transduced cells. Cells were treated with E7107 (0.5 nM) or DMSO in 96-well plate format and were changed into fresh medium containing E7107 or DMSO every 2 d. Relative cell growth was assessed on day 6 after E7107 exposure using the LSR Canto.

Overexpression of the *SF3B1*^{WT} or *SF3B1*^{R1074H} allele was introduced into *MLL–AF9*;*Srsf2*$^{P95H/+}$ leukemic cells using the PiggyBac transposon system (**Supplementary Fig. 5e**). 2 μg of PiggyBac Transposase construct (CMV-PB-Transposase-IRES-TK-HSV) and 6 μg of either the *SF3B1*^{WT} (ITR-CAG-Flag-*SF3B1*^{WT}-IRES-Puro-ITR) or the *SF3B1*^{R1074H} (ITR-CAG-Flag-*SF3B1*^{R1074H}-IRES-Puro-ITR) cDNA construct were electroporated into 2 × 10^6 cells (in a 200-μl volume) using the Amaxa Nucleofector Protocol (Program T-003) according to the manufacturer's instructions (Lonza). Puromycin selection (1 μg/ml) was initiated 4 d after electroporation to select for cells that successfully incorporated the constructs. Sanger sequencing was performed to confirm successful integration of the cDNA plasmid using the primers Fwd: TCCAATCAAAGATCTTCTTCCAA and Rev: GAGCAGGTTTCTGCAACGAT.

***In vitro* cell viability assays.** Cells were seeded in white flat-well 96-well plates (Costar) at a density of 10,000 cells per well. ATP luminescence readings were taken 48 h after E7107 treatment using Cell Titer Glo (Promega) according to the manufacturer's instructions.

Semi-quantitative and quantitative RT–PCR. Total RNA was isolated using the RNeasy Mini or Micro Kit (Qiagen). For cDNA synthesis, total RNA was reverse-transcribed with the SuperScript VILO cDNA Synthesis kit (Life Technologies). Primers used in the RT–PCR reactions were: *Dot1l* (exons 11–13), Fwd: ACTTGAGTGACATTGGCACCA, Rev: AGCACCAGAATCCGCGGGG; *Meis1* (exons 7–9), Fwd: CGGCATCCACTCGTTCAG, Rev: TCACTTGAAG GATGGTAAGTCCT; *Gapdh*, Fwd: CCATGACAACTTTGGCATTG, Rev: CCTG CTTCACCACCTTCTTG; *EZH2* (exons 9–10), Fwd: TTTCATGCAACA CCCAACACT, Rev: CCCTGCTTCCCTATCACTGT. The PCR cycling conditions chosen were as follows: 33 cycles of (i) 45 s at 95 °C; (ii) 45 s at 52 °C; (iii) 60 s at 72 °C; with a subsequent 5-min extension at 72 °C. Reaction products were analyzed on 2% agarose gels. The bands were visualized by ethidium bromide staining.

Quantitative RT–PCR (qRT–PCR) analysis was performed on an Applied Biosystems QuantStudio 6 Flex cycler using Power SYBR Green PCR Master Mix (ThermoFisher Scientific). The following primers were used: *EZH2* inclusion, Fwd: CAGCATTTGCCACTCCTACC, Rev: AGAGCAGCAGCAAACTCCTTT; *EZH2* exclusion,c Fwd: CAGCATTTGGAGGGAGCA, Rev: GCTGGGC CTGCTACTGTTATT; 18S rRNA, Fwd: GTAACCCGTTGAACCCCATT, Rev: CCATCCAATCGGTAGTAGCG; *Dot1l* exclusion, Fwd: GCAGGAAC TTGAGTGCTTGAA, Rev: GGCAGCTGCTTTGCTCTC; *Dot1l* inclusion, Fwd: CGGCAGAATCGTATCCTCAA, Rev: AAGTATGGTGCGGTCAATG; *Meis1* exclusion, Fwd: TAACAGCAGTGAGCAAGCAC, Rev: AATAAACCAATTG TTCACTTGAAGG; *Meis1* inclusion, Fwd: AAGGTGATGGCTTGGACAAC, Rev: AGGGTGTGTTAGATGCTGGAA; *Gapdh*, Fwd: TGGAGAAACCT GCCAAGTATG, Rev: GGAGACAACCTGGTCCTCAG.

All samples, including the template controls, were assayed in triplicate. The relative number of target transcripts was normalized to the housekeeping gene found in the same sample. The relative quantification of target gene expression was performed with the standard curve or comparative cycle threshold (C_T) method.

Statistical analyses. Statistical significance was determined by Student's *t*-test or analysis of variance (ANOVA) after testing for normal distribution. For Kaplan–Meier survival analysis, Mantel–Cox log-ranked test was used to determine statistical significance. Data were plotted as mean values with error bars representing s.d. using GraphPad Prism 7 software.

Targeted genomic sequencing using MSKCC IMPACT. Genomic alterations from FACS-purified hCD45$^+$ BM cells from NSG mice of PDX models were profiled using the MSKCC IMPACT assay as described previously[33]. Genomic DNA was extracted using DNeasy Blood and Tissue Kit (Qiagen).

Replicates. RNA-seq was conducted with 3–5 biological replicates from each group. Genetic phenotyping experiments were replicated three times independently. For *in vivo* experiments, the number of animals was chosen to ensure 90% power with 5% error based on observed s.d. Flow cytometric experiments were replicated independently two or three times. Pilot studies were conducted with drug studies, and results were replicated in a larger study to achieve enough statistical power. *In vitro* experiments were replicated two or three times, and viability experiments were completed in triplicate.

mRNA isolation, sequencing, and analysis. RNA was extracted from sorted mouse cell populations using Qiagen RNeasy columns. Poly(A)-selected, unstranded Illumina libraries were prepared with a modified TruSeq protocol. 0.5× AMPure XP beads were added to the sample library to select for fragments <400 bp, followed by addition of 1× beads to select for fragments >100 bp. These fragments were then amplified with PCR (15 cycles) and separated by gel electrophoresis (2% agarose). 300-bp DNA fragments were isolated and sequenced on the Illumina HiSeq 2000 (~100 million 101-bp reads per sample).

Publicly available RNA-seq data. Unprocessed RNA-seq reads from 31 patients with AML (with *MLL* rearrangements) were downloaded from the US National Center for Biotechnology Information (NCBI) sequence read archive (SRA; accession numbers SRP028594, SRP033266, SRP048759, and SRP056295). The data consisted of paired-end 2 × 100-bp libraries, with an average read count of 102 million per sample. The *SRSF2* mutational status of the samples was obtained from Lavallée *et al.*[16].

Genome annotations. To create organism-specific gene and genome annotation files, information was combined across University of California, Santa Cruz (UCSC) and Ensembl databases, using mouse assembly mm10 (NCBI GRCm38) and human assembly hg19 (NCBI GRCh37). To create splice junction annotation files, alternatively spliced cassette exons, competing 5′ or 3′ splice sites, and retained introns were obtained from MISO v2.0 (ref. 13). Constitutively spliced exons and introns were identified based on exon–exon junctions that were not alternatively spliced according to UCSC knownGene[34]. Novel junctions were defined from the UCSC and Ensembl 71 databases[35] using all possible combinations of splice sites, as described previously[36].

RNA-seq read mapping. All human and mouse samples were processed using the same pipeline. (i) The reads were mapped to their respective genome

doi:10.1038/nm.4097

assembly, using Bowtie v1.0.0 (ref. 37) and RSEM v.1.2.4 (ref. 38). The latter was internally modified to call Bowtie with -v 2, and it was run on the gene annotation file with the parameters --bowtie-m 100 --bowtie-chunkmbs 500 --calc-ci --output-genome-bam. (ii) BAM files from step 1 were filtered to remove reads in which the alignment mapq score was 0 and the splice junction overhang was <6 nt. (iii) All remaining unaligned reads were mapped to the splice junction annotation files using TopHat v2.0.8b (refs. 39,40), called with the parameters --bowtie1 --read-mismatches 3 -- read-edit-dist 2 --no-mixed --no-discordant --min-anchor-length 6 --splice-mismatches 0 --min-intron-length 10 --max-intron-length 1000000 --min-isoform-fraction 0.0 --no-novel-juncs --no-novel-indels --raw-juncs. The --mate-inner-dist and --mate-std-dev arguments were calculated using the MISO exon_utils.py script, which maps reads to constitutively spliced exon junctions. (iv) The reads aligned to splice junctions were filtered as in ii. (v) All resulting BAM files were merged to create a combined file of all aligned RNA-seq reads.

Identification and quantification of differential splicing. Isoform ratios for all alternative splicing events were quantified using MISO v2.0 (ref. 13). Constitutively spliced exons and introns were quantified using junction-spanning reads, as previously described[36]. The conditional knock-in and knockout mice were compared in a pair-wise manner, and for each pair the analysis was restricted to splicing events with 20 or more reads supporting either or both isoforms, and for which the event was alternatively spliced in the sample pair. From that subsets of events, those that fulfilled the following criteria were defined as differentially spliced: (i) they had at least 20 relevant reads in both samples, (ii) the change in absolute isoform ratio was ≥ 10%, and (iii) the statistical analysis of isoform ratios had a Bayes factor ≥5, when calculated using Wagenmakers's framework[14]. The human AML samples were analyzed by calculating the median isoform ratios across all 28 *SRSF2*$^{+/+}$ samples and comparing those in a pair-wise manner to each sample with mutated *SRSF2*, using the same methodology as for the knock-in and knockout mice. The *Mx1-Cre*$^{+}$*Srsf2*$^{+/+}$ or *Mx1-Cre*$^{+}$*Srsf2*$^{P95H/+}$ E7107-treated mice were compared in a pair-wise manner against the median isoform ratios of their vehicle-treated counterparts, using the same methodology. For the *MLL–AF9*-AML-transformed mice, there were sufficient numbers of replicates to do a group-based comparison within the *Srsf2*^{P95H} and *Srsf2*$^{+/+}$ genotypes individually ($n = 5$ for each genotype–treatment combination). E7107- and vehicle-treated mice were compared in a two-sided Wilcoxon rank-sum test, using the total number of isoform reads within each treatment group. Events were categorized as being differentially spliced if they fulfilled the following criteria: (i) they had at least 20 relevant reads in both samples, (ii) the change in median absolute isoform ratio was ≥10%, and (iii) they had a P value <0.01.

Gene expression analysis. All comparisons of gene expression levels were performed using RNA-seq read counts normalized with the trimmed mean of M values (TMM) method[41]. The scaling factors were calculated based on protein-coding genes only. For comparisons with fewer than five replicates per group, we used Wagenmakers's Bayesian framework[14] to compare samples in a pair-wise manner, as described above for the analysis of differential splicing. Differentially expressed genes had to have a Bayes factor >100. For the *MLL–AF9* leukemic mouse model, E7107- and vehicle-treated mice within the *Srsf2*$^{+/+}$ or *Srsf2*$^{P95H/+}$ genotype were analyzed using a two-sided Wilcoxon rank-sum test to compare the five replicates within each genotype–treatment group. Differentially expressed genes had to fulfill the following criteria: (i) a difference in abundance greater than a fold change of 2, and (ii) a P value <0.01.

Gene Ontology (GO) enrichment analysis. For each genotype–treatment comparison, we identified genes that were differentially expressed in at least one of the replicates to test for enrichment of GO biological process terms using the R package goseq[42]. All protein-coding genes were included as the background gene set. The 'Wallenius' method was used, and the resulting false-discovery rates were corrected using the Benjamini–Hochberg approach. Only terms with at least two ancestors were tested, and terms with more than 500 genes associated with them were removed to eliminate parent terms associated with generic biological processes.

Motif enrichment and distribution. The relative occurrences of sequence motifs in exons with increased inclusion versus exclusion rates in a given sample comparison were calculated. For the analysis of E7107 treatment in *Srsf2*$^{+/+}$ or *Srsf2*$^{P95H/+}$ mutant mice in the *Mx1-Cre* model, exons with decreased inclusion rates were compared to all exons with no changes in splicing, as the number of exons with increased inclusion rates was insufficient for statistical analysis. The 95% confidence interval for the enrichment ratios were computed based on bootstrapping, using 500 resampling steps for the enrichment ratios, or 100 steps for displaying the spatial distribution of motifs along a meta-exon.

Sample clustering. *MLL–AF9*-AML-transformed mice were clustered using multidimensional scaling (also known as principal coordinates analysis) of distances calculated using the 'canberra' method, $\text{sum}(|x_i - y_i|/|x_i + y_i|)$. For cassette exons and retained introns, only events that were alternatively spliced in the samples and had more than 20 reads in at least one sample were included. For protein-coding genes only genes with normalized expression >10 in at least one sample were included. Hierarchical clustering was performed on z-score-standardized data with the 'ward.D2' method, using the most variable splicing events and genes across samples (s.d. across the 20 mice > 0.25; splicing event or gene could be detected in at least ten mice).

Mouse versus human splicing comparison. For the cumulative distribution function (CDF) comparison of cassette exon-splicing and intron retention in *MLL–AF9* myeloid leukemias following *in vivo* E7107 or vehicle treatment, only cassette exons and introns within mouse homologs of genes containing differentially spliced events in at least one of the human *SRSF2 MLL*-rearranged AML samples were included.

Mouse homologs of the differentially spliced human genes were extracted from the Ensembl database version 81 (ref. 43) using BioMart.

30. National Research Council. *Guide for the Care and Use of Laboratory Animals* 8th edn. (The National Academies Press, 2011).
31. Wang, H.Y., Xu, X., Ding, J.H., Bermingham, J.R. Jr. & Fu, X.D. SC35 plays a role in T cell development and alternative splicing of *CD45*. *Mol. Cell* **7**, 331–342 (2001).
32. Georgiades, P. *et al. Vav-Cre* transgenic mice: a tool for mutagenesis in hematopoietic and endothelial lineages. *Genesis* **34**, 251–256 (2002).
33. Cheng, D.T. *et al.* Memorial Sloan Kettering–integrated mutation profiling of actionable cancer targets (MSK-IMPACT): a hybridization-capture-based next-generation sequencing clinical assay for solid tumor molecular oncology. *J. Mol. Diagn.* **17**, 251–264 (2015).
34. Meyer, L.R. *et al.* The UCSC Genome Browser database: extensions and updates 2013. *Nucleic Acids Res.* **41**, D64–D69 (2013).
35. Flicek, P. *et al.* Ensembl 2013. *Nucleic Acids Res.* **41**, D48–D55 (2013).
36. Hubert, C.G. *et al.* Genome-wide RNAi screens in human brain tumor isolates reveal a novel viability requirement for *PHF5A*. *Genes Dev.* **27**, 1032–1045 (2013).
37. Langmead, B., Trapnell, C., Pop, M. & Salzberg, S.L. Ultrafast and memory-efficient alignment of short DNA sequences to the human genome. *Genome Biol.* **10**, R25 (2009).
38. Li, B. & Dewey, C.N. RSEM: accurate transcript quantification from RNA-seq data with or without a reference genome. *BMC Bioinformatics* **12**, 323 (2011).
39. Kim, D. *et al.* TopHat2: accurate alignment of transcriptomes in the presence of insertions, deletions and gene fusions. *Genome Biol.* **14**, R36 (2013).
40. Trapnell, C., Pachter, L. & Salzberg, S.L. TopHat: discovering splice junctions with RNA-seq. *Bioinformatics* **25**, 1105–1111 (2009).
41. Robinson, M.D. & Oshlack, A. A scaling normalization method for differential expression analysis of RNA-seq data. *Genome Biol.* **11**, R25 (2010).
42. Young, M.D., Wakefield, M.J., Smyth, G.K. & Oshlack, A. Gene ontology analysis for RNA-seq: accounting for selection bias. *Genome Biol.* **11**, R14 (2010).
43. Guberman, J.M. *et al.* BioMart central portal: an open database network for the biological community. *Database* **2011**, bar041 (2011).

Corrigendum: Retinal lipid and glucose metabolism dictates angiogenesis through the lipid sensor Ffar1

Jean-Sébastien Joyal, Ye Sun, Marin L Gantner, Zhuo Shao, Lucy P Evans, Nicholas Saba, Thomas Fredrick, Samuel Burnim, Jin Sung Kim, Gauri Patel, Aimee M Juan, Christian G Hurst, Colman J Hatton, Zhenghao Cui, Kerry A Pierce, Patrick Bherer, Edith Aguilar, Michael B Powner, Kristis Vevis, Michel Boisvert, Zhongjie Fu, Emile Levy, Marcus Fruttiger, Alan Packard, Flavio A Rezende, Bruno Maranda, Przemyslaw Sapieha, Jing Chen, Martin Friedlander, Clary B Clish & Lois E H Smith
***Nat. Med.*; doi:10.1038/nm.4059; corrected 24 March 2016**

In the version of this article initially published online, there were two errors. There was a typographical error in the text, which should have stated that the 'dark current' is an electrochemical gradient required for photon-induced polarization (rather than depolarization, as incorrectly stated). In addition, some funding sources were inadvertently omitted from the Acknowledgments. The errors have been corrected for the print, PDF and HTML versions of this article.

Corrigendum: ROR-γ drives androgen receptor expression and represents a therapeutic target in castration-resistant prostate cancer

Junjian Wang, June X Zou, Xiaoqian Xue, Demin Cai, Yan Zhang, Zhijian Duan, Qiuping Xiang, Joy C Yang, Maggie C Louie, Alexander D Borowsky, Allen C Gao, Christopher P Evans, Kit S Lam, Jianzhen Xu, Hsing-Jien Kung, Ronald M Evans, Yong Xu & Hong-Wu Chen
***Nat. Med.*; doi:10.1038/nm.4070; corrected online 22 April 2016**

In Figure 2a of the version of this article initially published online, one phenyl ring was inadvertently deleted from the chemical structure of compound SR2211. One affiliation of H.-W.C. (Veterans Affairs Northern California Health Care System–Mather, Mather, California, USA) was also inadvertently omitted. These errors have been corrected for the print, PDF and HTML versions of this article.

Corrigendum: Protection against malaria at 1 year and immune correlates following PfSPZ vaccination

Andrew S Ishizuka, Kirsten E Lyke, Adam DeZure, Andrea A Berry, Thomas L Richie, Floreliz H Mendoza, Mary E Enama, Ingelise J Gordon, Lee-Jah Chang, Uzma N Sarwar, Kathryn L Zephir, LaSonji A Holman, Eric R James, Peter F Billingsley, Anusha Gunasekera, Sumana Chakravarty, Anita Manoj, MingLin Li, Adam J Ruben, Tao Li, Abraham G Eappen, Richard E Stafford, Natasha K C, Tooba Murshedkar, Hope DeCederfelt, Sarah H Plummer, Cynthia S Hendel, Laura Novik, Pamela J M Costner, Jamie G Saunders, Matthew B Laurens, Christopher V Plowe, Barbara Flynn, William R Whalen, J P Todd, Jay Noor, Srinivas Rao, Kailan Sierra-Davidson, Geoffrey M Lynn, Judith E Epstein, Margaret A Kemp, Gary A Fahle, Sebastian A Mikolajczak, Matthew Fishbaugher, Brandon K Sack, Stefan H I Kappe, Silas A Davidson, Lindsey S Garver, Niklas K Björkström, Martha C Nason, Barney S Graham, Mario Roederer, B Kim Lee Sim, Stephen L Hoffman, Julie E Ledgerwood & Robert A Seder, for the VRC 312 and VRC 314 Study Teams
***Nat. Med.*; doi:10.1038/nm.4110; corrected online 18 May 2016**

In the version of this article initially published online, the authors omitted a funding source, The Bill and Melinda Gates Foundation (Investment ID: 24922). The error has been corrected for the print, PDF and HTML versions of this article.

Erratum: Modulation of splicing catalysis for therapeutic targeting of leukemia with mutations in genes encoding spliceosomal proteins

Stanley Chun-Wei Lee, Heidi Dvinge, Eunhee Kim, Hana Cho, Jean-Baptiste Micol, Young Rock Chung, Benjamin H Durham, Akihide Yoshimi, Young Joon Kim, Michael Thomas, Camille Lobry, Chun-Wei Chen, Alessandro Pastore, Justin Taylor, Xujun Wang, Andrei Krivtsov, Scott A Armstrong, James Palacino, Silvia Buonamici, Peter G Smith, Robert K Bradley & Omar Abdel-Wahab
***Nat. Med.*; doi:10.1038/nm.4097; corrected 11 May 2016**

In the version of this article initially published online, the graphs in Figure 3b–d were laid out incorrectly and were not consistent with the figure legend and text. The error has been corrected for the print, PDF and HTML versions of this article.